AFRL-RX-WP-TP-2011-4297

A NEUTRON AND X-RAY DIFFRACTION STUDY OF Ca-Mg-Cu METALLIC GLASSES (Preprint)

Daniel B. Miracle

Metals Branch
Metals, Ceramics, and NDE Division

Emma R. Barney and Alex C. Hannon

Rutherford Appleton Laboratory, ISIS Facility

Oleg N. Senkov and James M. Scott

UES, Inc.

Robert M. Moss

University of Kent, School of Physical Sciences

JULY 2011

AIR FORCE RESEARCH LABORATORY
MATERIALS AND MANUFACTURING DIRECTORATE
WRIGHT-PATTERSON AIR FORCE BASE, OH 45433-7750
AIR FORCE MATERIEL COMMAND
UNITED STATES AIR FORCE

REPORT DOCUMENTATION PAGE

Form Approved
OMB No. 0704-0188

1. REPORT DATE *(DD-MM-YY)*	2. REPORT TYPE	3. DATES COVERED *(From - To)*
July 2011	Journal Article Preprint	01 July 2011 – 01 July 2011

4. TITLE AND SUBTITLE
A NEUTRON AND X-RAY DIFFRACTION STUDY OF Ca-Mg-Cu METALLIC GLASSES (Preprint)

5a. CONTRACT NUMBER
In-House

5b. GRANT NUMBER

5c. PROGRAM ELEMENT NUMBER
62102F

6. AUTHOR(S)
Daniel B. Miracle (Metals, Ceramics, and NDE Division, Metals Branch (AFRL/RXLM))
Emma R. Barney and Alex C. Hannon (Rutherford Appleton Laboratory, ISIS Facility)
Oleg N. Senkov and James M. Scott (UES, Inc.)
Robert M. Moss (University of Kent, School of Physical Sciences)

5d. PROJECT NUMBER
4347

5e. TASK NUMBER
20

5f. WORK UNIT NUMBER
LM10512P

7. PERFORMING ORGANIZATION NAME(S) AND ADDRESS(ES)

Metals, Ceramics, and NDE Division, Metals Branch (AFRL/RXLM)
Materials and Manufacturing Directorate
Air Force Research Laboratory
Wright-Patterson Air Force Base, OH 45433-7750
Air Force Materiel Command, United States Air Force

- Rutherford Appleton Laboratory, ISIS Facility
- UES, Inc.
- University of Kent, School of Physical Sciences

8. PERFORMING ORGANIZATION REPORT NUMBER
AFRL-RX-WP-TP-2011-4297

9. SPONSORING/MONITORING AGENCY NAME(S) AND ADDRESS(ES)
Air Force Research Laboratory
Materials and Manufacturing Directorate
Wright-Patterson Air Force Base, OH 45433-7750
Air Force Materiel Command
United States Air Force

10. SPONSORING/MONITORING AGENCY ACRONYM(S)
AFRL/RXLM

11. SPONSORING/MONITORING AGENCY REPORT NUMBER(S)
AFRL-RX-WP-TP-2011-4297

12. DISTRIBUTION/AVAILABILITY STATEMENT
Approved for public release; distribution unlimited.

13. SUPPLEMENTARY NOTES
PAO case number 88ABW-2010-6303, cleared 30 November 2010. The U.S. Government is joint author of this work and has the right to use, modify, reproduce, release, perform, display, or disclose the work. Submitted to Intermetallics Review.

14. ABSTRACT
The structures of $Ca_{60}Mg_{15}Cu_{25}$, $Ca_{60}Mg_{20}Cu_{20}$ and $Ca_{60}Mg_{25}Cu_{15}$ metallic glasses have been investigated by neutron and X-ray diffraction. The correlation functions show a peak manifold in the region 2.2 Å to 4.5 Å, arising from the various atom pairs for these glasses. The results show clearly that there are contacts between the solute atoms (Cu and Mg) in agreement with a simple estimate of the maximum solute atom fraction beyond which solute-solute contact becomes topologically necessary. The Cu-Mg and Cu-Ca distances are consistent with the sum of covalent radii, whereas all other interatomic distances are consistent with the sum of metallic radii. The neutron and X-ray diffraction correlation functions were simultaneously fitted with a series of symmetric peaks to obtain coordination numbers and interatomic distances, but only the results from the first two peaks, Cu-Cu and Cu-Mg, are of reasonable reliability. The Percus-Yevick approximation for binary hard sphere systems has been used to simulate the results.

15. SUBJECT TERMS
ternary alloy systems, glasses, metallic, rapid solidification processing, diffraction

16. SECURITY CLASSIFICATION OF:			17. LIMITATION OF ABSTRACT:	18. NUMBER OF PAGES	19a. NAME OF RESPONSIBLE PERSON (Monitor)
a. REPORT	b. ABSTRACT	c. THIS PAGE			Jonathan Spowart
Unclassified	Unclassified	Unclassified	SAR	42	19b. TELEPHONE NUMBER *(Include Area Code)* N/A

A neutron and X-ray diffraction study of Ca-Mg-Cu metallic glasses

Emma R. Barney [b*], *Alex C. Hannon* [b], *Oleg N. Senkov* [a,c], *James M. Scott* [a,c], *Daniel B. Miracle* [a] *and Robert M. Moss* [d]

[a] Air Force Research Laboratory, Materials and Manufacturing Directorate, Wright-Patterson AFB, OH 45433, USA

[b] ISIS Facility, Rutherford Appleton Laboratory, Chilton, Didcot, OX11 0QX, UK.

[c] UES, Inc., 4401 Dayton-Xenia Road, Dayton, OH 45432, USA

[d] School of Physical Sciences, University of Kent, Canterbury, CT2 7NH, UK

* Corresponding author, Emma.Barney@stfc.ac.uk. Telephone number: 01235 446588. Fax number: 01235 445720

Abstract

The structures of $Ca_{60}Mg_{15}Cu_{25}$, $Ca_{60}Mg_{20}Cu_{20}$ and $Ca_{60}Mg_{25}Cu_{15}$ metallic glasses have been investigated by neutron and X-ray diffraction. The correlation functions show a peak manifold in the region 2.2 Å to 4.5 Å, arising from the various atom pairs for these glasses. The results show clearly that there are contacts between the solute atoms (Cu and Mg) in agreement with a simple estimate of the maximum solute atom fraction beyond which solute-solute contact becomes topologically necessary. The Cu-Mg and Cu-Ca distances are consistent with the sum of covalent radii, whereas all other interatomic distances are consistent with the sum of metallic radii. The neutron and X-ray diffraction correlation functions were simultaneously fitted with a series of symmetric peaks to obtain coordination numbers and interatomic distances, but only the results from the first two peaks, Cu-Cu and Cu-Mg, are of reasonable reliability. The Percus-Yevick approximation for binary hard sphere systems has been used to simulate the results. This shows that the results of fits to the Cu-Cu and Cu-

Mg correlations give a reasonable description for atoms which are in close contact, but do not include an additional contribution at longer distance due to atoms which are almost in contact. The fits to the Cu-Ca peak are strongly affected by overlaps with both the longer distance peaks used in the fit, and the broad trailing edge in the distributions of interatomic distances that is not taken into account by fitting with symmetric peaks. Final results show that copper has a total of 6.5 neighbours which are in close contact, but has a total coordination number of about 12-13, when atoms which are almost in contact are included.

Keywords: A. Ternary alloy systems; B. Glasses, metallic; C. Rapid solidification processing; F. Diffraction

1 Introduction

Metallic glasses have a wide range of potential applications due to their magnetic properties, high yield strength, low elastic modulus and corrosion resistance. The earliest reports of metallic glasses were for compositions which required extreme cooling rates to form minute quantities [1], but since that time many compositions have been reported which can be quenched at a slower cooling rate to form bulk amorphous materials. This has allowed the unique properties of amorphous metals to be utilised in the development of a wide range of products, including small scale devices, such as micro-electro-mechanical systems (MEMS) [2,3]. Despite a wide range of current and potential technological applications, a detailed understanding of the link between the structures of glasses, the glass forming abilities and the physical properties they exhibit has not been reached and, although models for the structure of binary glasses have been proposed, the structure of more complicated amorphous systems is still not well understood.

A number of structural studies of bulk metallic glasses have been carried out using both X-ray and neutron diffraction, as well as by applying modelling methods such as Reverse Monte Carlo (RMC) and molecular dynamics (MD). Significant progress has been made in understanding the structure of binary metallic glasses using these methods, and the results indicate that the packing of atoms in these materials is not random, but is strongly influenced by chemical interactions. In the case of $Ni_{81}B_{19}$, for

example, there is a strong preference for unlike-atom bonds, and there are no B-B nearest neighbours at all [4]. These studies have resulted in the formulation of the efficient cluster packing (ECP) model [5]. In this model, the simplest case is one for which the solute atom (B in the case of $Ni_{81}B_{19}$) is relatively dilute in the alloy, and all the nearest neighbours are solvent atoms (Ni atoms). In the literature, there are many examples of glasses for which this solute-lean model is applicable, including $Ni_{81}B_{19}$ [4], $F_{80}B_{20}$ [6], $Ti_{84}Si_{22}$ [7] and $Co_{80}P_{20}$ [8]. However, many of the bulk metallic glasses which exhibit the modest cooling rates and large critical diameters necessary for bulk applications are complex systems containing three or more atom types, and with solvent concentrations that are too low to allow each solute atom to be surrounded only by the solvent. Instead, following the idea of the ECP model for solute rich glasses [9], solute atoms must substitute onto solvent atom sites. It is thought that the more complex structure this produces is the cause of the increased glass forming ability (GFA) of these materials because, coupled with the high density, and therefore low free volume of a bulk metallic glass [10,11], it is much harder for the atoms to rearrange to form a crystalline structure [3]. These solvent anti-site defects can also increase the number of unlike atom bonds, further increasing the stability [9]. Senkov *et al.* [12-16] have published several papers on the GFA and physical properties of the glass systems $Ca_xMg_yCu_{(100-(x+y))}$, $Ca_xMg_yZn_{(100-(x+y))}$ and $Ca_xMg_yZn_zCu_{(100-(x+y+z))}$. These studies demonstrate that the GFA of the system is best for compositions where the solvent (Ca) accounts for approximately half the atoms. For example, the composition with the best GFA for the ternary system containing copper is $Ca_{50}Mg_{22.5}Cu_{27.5}$, where the critical thickness is 10 mm. This reduces rapidly as the amount of solvent (Ca) is increased, with samples containing $\geq$ 60 at.% Ca having a critical thickness of no more than 4 mm, reducing to $\leq$ 1mm for two compositions with 70 at.% Ca. Furthermore, the GFA is improved when the number of Cu and Mg atoms in the system are similar, or when the composition includes slightly more copper atoms. This suggests that good GFA in this system is a balance between having as many atoms of each of the three elements as possible, and having a large number of atoms of copper, which has a significantly smaller radius than calcium and magnesium (see Table 1). This maximises the complexity of the structure, in line with the empirical rules for high GFA laid down by Inoue [17,18].

The interpretation of diffraction results for metallic glass systems which contain more than two atom types is challenging. The atomic radii of the elements involved are often distributed such that the first peaks of the partial correlation functions overlap and the determination of individual interatomic distances from the total correlation function, *T(r)*, is extremely difficult. A common approach is to use modelling techniques, such as RMC, where models are constructed to fit reciprocal space data, and then interatomic distances and partial coordination numbers are calculated from the model. A recent RMC study of the related Ca-Mg-Zn glass system has given insights into the changes in glass structure with composition, and how this affects the GFA, encouraging crystallisation [16]. The direct approach for extracting information on the short range order in the glass is to fit peaks to the correlation function, *T(r)*, but for ternary glasses there are six independent partial pair correlation functions which, in principle, require six independent experiments with different elemental weighting factors for a unique separation of partial functions. Nonetheless, the fitting method has been applied successfully to the ternary glass system $Al_{90}Fe_xCe_{10-x}$ [21,22], where the compositions are favourable for the fitting technique due to the low concentration of iron and cerium in these samples. *T(r)* is dominated by aluminium correlations and, if Fe and Ce are considered together as the solute, then the ECP model indicates that there will be no Fe-Fe, Ce-Ce and Fe-Ce nearest neighbours. Therefore, the fit was reduced to three peaks and the environments of all three elements were measured reliably. The work carried out on the systems $Zr_{70}Al_{10}(Ni, Cu)_{20}$ [23,24] is more relevant because the concentration of solute atoms is comparable to the glasses studied here. The multiple peak fitting technique was applied to the X-ray and neutron correlation functions with some success and it was demonstrated, with additional information from Zr, Ni, and Cu EXAFS, that the addition of aluminium has a large impact on the glass structure when substituted into the binary glasses $Zr_{70}(Ni,Cu)_{30}$. The Zr environment was determined for both glasses, though again the solute-solute correlations were neglected.

In this study the structure of the glass system, $Ca_{60}Mg_{40-x}Cu_x$, is examined by using direct fitting of total correlation functions, *T(r)*, measured using both neutron and X-ray diffraction. For this method there are difficulties which arise from the large number of overlapping contributions, and the fact that

there is insufficient information for an unambiguous separation of partials. However, it is demonstrated that important structural insights can be gained by using this method, even in cases where solute-solute correlations cannot be neglected, provided that the analysis is carried out in a critical manner, and with reasonable constraints applied to the peak positions for the various correlations. To assess the reliability of the coordination numbers extracted, the data are compared to partial correlation functions, $t_{ll'}(r)$, calculated using the Percus-Yevick (PY) approximation for a binary hard sphere system [25,26].

2 X-ray and neutron diffraction theory

A total scattering experiment measures the total (X-ray or neutron) scattering from the sample, $I(Q)$, where Q is the magnitude of the scattering vector for elastic scattering [27]. The total scattering is the sum of the self-scattering, $I^s(Q)$ (the interference between waves scattered from the same atom), and the distinct scattering, $i(Q)$ (the interference between waves scattered from different atoms), which is expressed simply for neutron diffraction as a differential cross-section:

$$\frac{d\sigma}{d\Omega} = I^{\mathrm{N}}(Q) = I^s(Q) + i^{\mathrm{N}}(Q) \qquad (1)$$

For both X-rays and neutrons, the self-scattering can be calculated within an approximation for a sample of known composition, and is subtracted from the data to give the distinct scattering.

For neutron diffraction, $i^{\mathrm{N}}(Q)$, can then be Fourier transformed to give a real-space correlation function,

$$T^{\mathrm{N}}(r) = 4\pi\rho^0 r\left(\sum_i c_\iota \bar{b_\iota}\right)^2 + \frac{2}{\pi}\int_0^\infty Q i^{\mathrm{N}}(Q) M(Q)\sin(rQ)\,dQ \qquad (2)$$

where $M(Q)$ is a modification function which is used to reduce termination ripples in the Fourier transform. ρ^0 is the atomic number density, and c_ι and $\bar{b_\iota}$ are respectively the atomic fraction and

coherent neutron scattering length for element l. The resolution in real-space depends on the modification function, and principally on the maximum momentum transfer, Q_{max}, of the experimental data.

In the case of X-ray diffraction, the situation is more complex because X-rays scatter from the electron cloud, yielding a relatively broad 'electron-electron' correlation function. To account for this, the sharpened distinct scattering is obtained by first dividing by $\langle f(Q)\rangle^2$ (where $\langle f(Q)\rangle$ is the mean X-ray form factor for the sample) [28,29], to approximate scattering from point sources;

$$i^{\mathrm{X}}(Q) = \frac{I^{\mathrm{X}}(Q) - \langle f(Q)^2\rangle}{\langle f(Q)\rangle^2} \qquad (3)$$

The X-ray correlation function is then obtained according to

$$T^{\mathrm{X}}(r) = 4\pi\rho^0 r + \frac{2}{\pi}\int_0^\infty Q i^X(Q) M(Q)\sin(rQ)\, dQ \qquad (4)$$

The contribution to the distinct scattering due to a single interatomic distance, r_{jk}, with a root mean square (RMS) variation in distance of $\langle u_{jk}^2\rangle^{½}$ is

$$i_{jk}^{\mathrm{N}}(Q) = n_{jk} c_j \bar{b}_j \bar{b}_k \frac{sin(Qr_{jk})}{Qr_{jk}} exp\left(\frac{-\langle u_{jk}^2\rangle Q^2}{2}\right) \qquad (5)$$

$$i_{jk}^{\mathrm{X}}(Q) = n_{jk} c_j \frac{f_j(Q) f_k(Q)}{\langle f(Q)\rangle^2} \frac{sin(Qr_{jk})}{Qr_{jk}} exp\left(\frac{-\langle u_{jk}^2\rangle Q^2}{2}\right) \qquad (6)$$

where n_{jk} is the coordination number of k-type atoms around the atom j, and c_j is the atomic fraction for j-type atoms. The contribution to the correlation function due to the interatomic distance r_{jk} is then evaluated by Fourier transformation of $i_{jk}^{\mathrm{N}}(Q)$ or $i_{jk}^{\mathrm{X}}(Q)$, according to equation (2) or (4).

The coordination numbers for *j*-*k* and *k*-*j* atom pairs are related by the following identity

$$n_{jk} c_j = n_{kj} c_k. \qquad (7)$$

A coordination number only has meaning if the range in interatomic distances, r_{jk}, over which it applies, and the method by which it has been determined, is defined [30,31]. Provided that n_{jk} and n_{kj} have been determined over the same distance range, and by the same method, equation (7) is always true.

3 Experimental detail

Three samples of compositions, $Ca_{60}Mg_{15}Cu_{25}$, $Ca_{60}Mg_{20}Cu_{20}$ and $Ca_{60}Mg_{25}Cu_{15}$ were prepared by melt-spinning and characterised as described by Senkov *et al.* [13]

For neutron diffraction, small fragments of the sample were loaded into 10.3 mm diameter cylindrical vanadium containers, with walls which were 25 μm in thickness to reduce background scattering and absorption of neutrons by the container. The data were collected using the GEM diffractometer [32] at the ISIS pulsed neutron source at the Rutherford Appleton Laboratory, UK, and the data reduction, correction and analysis were carried out using a combination of the program GUDRUN [33] and the ATLAS suite of programs [34].

The X-ray diffraction data were collected on a Panalytical X'pert Pro Multi-Purpose Diffractometer which had been optimised for the study of disordered materials with a capillary stage for mounting the samples, and a tube with a silver anode for short wavelength X-rays (0.560885 Å). The samples were finely powdered and loaded in silica capillaries 1 mm in diameter and with walls of a nominal thickness of 0.01mm. The data were collected on a spinning sample for scattering angles over a range from 3.2° to 128° with 0.2° intervals. The data were corrected for multiple scattering, Compton scattering and bremsstrahlung effects, and normalised using a newly developed program, GudrunX [35].

Simultaneous fitting of the X-ray and neutron correlation functions, $T^X(r)$ and $T^N(r)$ was carried out using the program NXfit [36].

4 Results

The corrected neutron distinct scattering, $i^N(Q)$, for each of the three samples is shown in Figure 1(a), with expanded plots of the low Q region in Figure 2(a) and the neutron correlation function, $T^N(r)$, in Figure 3(a). For each figure, the X-ray diffraction data are shown in part (b), adjacent to the neutron data for comparison. $i^X(Q)$ for each of the three samples is shown in both Figure 1(b) and 2(b), whilst $T^X(r)$ is shown in Figure 3(b). The correlation functions were obtained by Fourier transformation, according to equations (2) and (4), using the Lorch modification function [37] with a maximum momentum transfer Q_{max} of 25 and 18 Å^{-1} for neutron and X-ray diffraction respectively. Differences between $T^N(r)$ and $T^X(r)$ provide more information on the various interatomic correlations in the glass than can be obtained by the use of one radiation alone.

The distinct scattering, $i(Q)$, for both radiations damps very quickly with Q and no oscillations are apparent beyond 15 Å^{-1} (see Figure 1), indicating that the glasses have a wide range of interatomic distances. However, small Bragg peaks in $i^N(Q)$ (at about 2.6 and 3.7 Å^{-1}) indicate that the samples are not completely amorphous. There is a small amount of crystallization for all three samples and the Bragg peak intensity increases as copper is added. The peaks have been identified as arising from CaO [38], which forms on the surface of the glasses (see Figure 2). The Bragg peaks are observed more clearly in the neutron diffraction patterns than in the X-ray diffraction patterns because the neutron diffraction measurement has a narrower resolution, and possibly also because neutrons are more penetrating. Figure 2 shows that there are systematic changes with composition in the distinct scattering which are consistent between the two radiations. As copper is substituted into the glass at the expense of magnesium, the first sharp diffraction peak (FSDP) shifts to higher Q and broadens. The correlation functions show that an increase in the Cu content causes a shortening of the average interatomic distance, and an increase in the width of the distribution of interatomic distances. Thus the shift of the FSDP may be interpreted as arising from the shortening of the average interatomic distance, whilst the broadening of the FSDP may arise from the broadening of the distribution of interatomic distances.

The correlation functions show a peak manifold in the region 2.2 Å to 4.5 Å, which arises from the interatomic distances between the various atom pairs in these glasses. Systematic changes with composition are also observed in the total correlation functions (see Figure 3). As the amount of copper in the sample is increased, there is an increase in area between 2.0 and 3.2 Å, and a corresponding decrease in area between 3.2 and 4.0 Å. Figure 4 shows the differences between the correlation functions with the two most disparate compositions ($Ca_{60}Mg_{15}Cu_{25}$ - $Ca_{60}Mg_{25}Cu_{15}$). The positions, r_{diff}, of the maxima and minima in the differences have been used to estimate the interatomic distances between different elements (see Table 2). For both radiations, the data for the sample with lower Cu content are subtracted from the data for the sample with higher Cu content, resulting in positive peaks arising from copper correlations, and negative peaks due to interatomic distances involving magnesium. The positions of the first three maxima and minima can be determined easily, because there is good agreement between the results from the two radiations and the features are well defined. At distances greater than 3 Å, although it is still possible to make an assignment of the interatomic distances, it is more difficult because the peaks are less distinct, with more variation between the differences measured by the two radiations. In Table 2 the bonding for each pair correlation is categorised as metallic or covalent, depending whether the value of r_{diff} is closer to the sum of metallic or covalent radii, r_{jk}^{M} or r_{jk}^{C}.

For each of the three samples, peak fits were simultaneously made to both $T^{N}(r)$ and $T^{X}(r)$ using the program NXfit [36]. The presence of three atom types with similar atomic radii (see Table 1) results in six different correlations with nearest neighbour distances between 2 and 4 Å (see Table 2), and it is impossible to deconvolute these six contributions by a unique fit to *T(r)*. However, by utilising the different scattering powers of the elements for the two radiations, and fitting the two correlation functions simultaneously, the range of possible fits to the data is drastically reduced. When this method of fitting is combined with the information on interatomic distances derived from the results in Figure 4, a final fit can be achieved which is a reasonable model for the short range order of the glass.

The initial simultaneous fit was made to the correlation functions for $Ca_{60}Mg_{15}Cu_{25}$. Five peaks were used to model each of the possible atom pairs, excluding Mg-Mg. Magnesium weakly scatters both X-rays and neutrons and this, coupled with the small number of magnesium atoms present in the three samples, leads to a contribution to *T(r)* from Mg-Mg distances which can be neglected without much effect on the measured coordination numbers for the other correlations. The initial positions for the five peaks were derived from the differences shown in Figure 4, and were then allowed to vary within limited bounds (± 0.05 Å), whilst the peak widths and areas were allowed to vary without constraint. The resultant fit was then used to provide the initial fit parameters for the fit to the $Ca_{60}Mg_{20}Cu_{20}$ data, and only the peak area (i.e. coordination number) was allowed to vary. This resulted in a poor fit in the region of the Mg-Ca and Ca-Ca correlations, and so the peak positions and widths of those peaks were then also allowed to vary. The final fitting parameters for this sample were then used in the same way as the starting parameters for the fit to the $Ca_{60}Mg_{25}Ca_{15}$ data. Figures 5-7 show the final fits to the X-ray and neutron data for each of the samples.

Once satisfactory fits to the X-ray and neutron datasets were achieved, the coordination numbers (and peak widths, where appropriate) for each sample were altered, and the program was allowed to refit the data. The differences between the final values for the two fits were then used as an estimate of the error. The fit parameters for the three correlations involving copper are given in Table 3. The Mg-Cu and Ca-Cu coordination numbers were calculated according to equation (7). The Mg-Ca and Ca-Ca peaks need to be included in the fits to improve the reliability of the fits to the copper peaks, but are significantly less reliable and are not reported. Figure **8** shows the variation with composition of the fitted coordination numbers for each of the copper correlations. Each coordination number appeared to vary linearly with copper content over the studied composition range.

5 Discussion

5.1 Peak fits and coordination numbers

There are suggestions, from both modelling studies [5,9] and experimental studies [23,24], that there may be no solute-solute contacts for ternary BMGs with low solute concentrations. The ECP model allows the number of structural sites to be counted [9], and so gives a formalism for calculating the maximum solute concentration where solute-solute contact can be avoided. Consider a Ca-Mg-Cu glass structure where all solute sites are occupied only by solute atoms and each solute site is surrounded only by solvent atoms. Using Mg as the primary structure-forming solute (α), the relative size of Mg and Ca atoms suggests that each α site will be surrounded by ~10 Ca atoms. Three additional solute sites occur at the interstices of these structure-forming α-centred clusters. There are thus a total of 14 structural sites per α site, and 4 of these are solute sites. The maximum solute atom fraction where solute-solute contact can be avoided is thus $4/14 \approx 0.29$. If α sites are primarily occupied by Cu atoms, then the number of Ca atoms surrounding each α site is ~9 and the critical solute concentration below which solute-solute contact may be avoided is $4/13 \approx 0.31$. Solute-solute contact becomes topologically necessary for solute concentrations greater than these values.

In agreement with this simple analysis, the correlation functions measured for the calcium-magnesium-copper system, shown in Figure 3, indicate that the glass structure in this system, which is comprised of 40% solute atoms, can only be explained if solute-solute contact occurs in these glasses. The complexity of the peak manifold between 2.2 and 4.5 Å, and the changes which occur on altering the relative amount of copper and magnesium with respect to calcium, indicate that there are more contributions than can arise from Cu-Ca, Mg-Ca, and Ca-Ca correlations alone. Thus, the solute-solute correlations Cu-Cu, Cu-Mg and Mg-Mg cannot be neglected. While glasses in the Ca-Mg-Cu system can be formed with compositions similar to $Zr_{70}Al_{10}(Ni, Cu)_{20}$ (i.e. $Ca_{70}(Mg,Cu)_{30}$), the GFA is poor [13]. This suggests that higher levels of solute, and solute-solute correlations, are beneficial to the formation of a BMG. This beneficial effect has been proposed to come from an increase in the more stable solute-solvent bonds that accompany an increase in the solute content [39].

The simultaneous fitting of the X-ray and neutron correlation functions achieves good agreement with the experimental data by using the interatomic distances identified from Figure 4 as a starting point. The narrow widths of the resolution-broadened Gaussian peaks modelling the Cu-Cu, Cu-Mg and Cu-Ca correlations (see Figures 5-7), are consistent with strong bonding of the copper. In contrast, the two fitted peaks for the Mg-Ca and Ca-Ca correlations are very broad and it was necessary to allow both the position and width of the peaks to vary between samples to achieve a better fit. Although broader peaks can be an indication of increased static disorder, it is likely that in this case the fitted peaks are not accurate representations of the distribution of Mg-Ca and Ca-Ca interatomic distances. Furthermore, extra area in the region of 3.2-4 Å may arise from a second shell of copper correlations (as in crystalline Ca_2Cu - see below), and therefore any attempts to extract structural information from the fits to the Mg-Ca and Ca-Ca peaks are less likely to yield reliable information. The consistency of the fits to the copper correlations indicates that realistic coordination numbers for copper can be measured over the limited range of ~2-3.2 Å and the fitting parameters for the copper related correlations are given in Table 3.

For a glass with a majority of calcium atoms, the coordination number for a minority atom can be calculated using both the dense random packing (DRP) model [40,41] and the ECP model [5,9]. For a calcium-based glass with minority copper atoms, both models indicate that the number of calcium nearest neighbours to a copper, n_{CuCa}, is between 8 and 9. In contrast, for a minority of copper atoms in a magnesium-based glass, both models result in a much higher copper coordination number of 10-12 because the radius of magnesium is significantly smaller than that of calcium. Therefore, the total Cu coordination number for the Ca-Mg-Cu ternary glass system would be expected to be between these two estimates. However, the total copper coordination number determined from the fits varies from 4.74 for the sample with the lowest copper content, to 5.74 for the sample containing the most copper; clearly this is significantly less than predicted by the DRP or ECP models.

The crystal structure of Ca_2Cu [42] can be considered as a binary crystalline analogue for the glass because it has a similar solute/solvent atom fraction. In this crystal a copper atom has 9 nearest neighbours closer than 3.5 Å (the longest Cu-Ca distance identified by the fits shown in Figures 5-7),

agreeing closely with the predictions of the DRP [40,41] and ECP models [5], though these models assume that all the neighbours are calcium while in the crystal there are two Cu neighbours, as shown in Figure 9. Furthermore, the average Cu-Ca distance is 3.07 Å, which is consistent with covalent bond lengths, and is much shorter than 3.24 Å, the average of the Cu-Cu (2.51Å) and Ca-Ca (3.98Å) distances. This is in good agreement with the interatomic distances, r_{diff} (Table 2), observed in Figure 4 and the non-additive nature of bond-lengths in BMGs has been discussed previously in a number of papers including one by Cheng et al. [43]. Figure 9 shows a comparison of the neutron correlation function for the glass ($Ca_{60}Mg_{15}Cu_{25}$) of closest composition to the crystal, with a simulation of the three contributions, Cu-Cu, Cu-Ca and Ca-Ca, based on the Ca_2Cu crystal structure [42]. For the simulation, the partial correlation functions for the crystal were calculated using the XTAL program [44], and were then weighted appropriately for the composition of the glass. The peak width used to broaden each of the partials was 0.15 Å, a typical value for the fits to the experimental data given in Table 3. The positions of the simulated Cu-Cu and Cu-Ca peaks are similar to those for the glass, but the peaks are too intense, indicating that the coordination numbers for Cu-Cu and Cu-Ca in the glass are significantly less than 2 and 7 respectively, in agreement with the fit results in Table 3.

It should be noted that the covalent Cu-Cu distance in Table 2 is unusual in that it is longer than the metallic distance. The tabulated covalent Cu radius was calculated as an average from a survey of many crystal structures [20]. This unusual behaviour may be related to the electronic structure of a copper atom, which has a single electron in the outermost orbital. This electron is donated to form metallic bonds and reduces the atomic radius to a greater extent than occurs when atoms overlap to form covalent bonds. The good agreement between the Cu-Mg and Cu-Ca distances calculated using the literature values for covalent radii and the distances determined from the diffraction data gives confidence that the values used for the covalent radii (notably for Cu) are reasonable.

If the packing were random, and not affected by chemical interactions, then the number of atoms of a certain type (X) around copper would be proportional to the total number of X atoms in the glass (i.e. proportional to the atomic fraction c_X), and similarly the number of Cu atoms around an X atom would be proportional to the total number of Cu atoms in the glass. The three Cu-X coordination

numbers for each sample (and the corresponding X-Cu coordination numbers, calculated according to equation (7)) are shown as a function of copper content in Figure 8. For all five coordination numbers, the changes with composition are significantly larger than the errors from varying the fitting of the data (indicated by error bars in Figure 8). Within errors, the solute-solute coordination numbers, are proportional to the relevant atomic fraction, so that $n_{CuCu}=(4.7\pm0.3)c_{Cu}$, $n_{MgCu}=(3.6\pm0.2)c_{Cu}$, and $n_{CuMg}=(3.6\pm0.2)c_{Mg}$, as indicated by the continuous lines in Figure 8. Thus the solute-solute coordination numbers derived from fitting a single symmetric peak to the experimental data behave in a way which is consistent with a random packing which is not affected by chemical interactions, i.e. with no preference for contact or avoidance of contact.

For the Ca-Cu coordination numbers, the continuous line in Figure 8 indicates a fit based on the assumption of proportionality to the Cu atom fraction, c_{Cu}; clearly the values of n_{CaCu} determined from fitting the experimental data are not proportional to c_{Cu}. (If the values of n_{CaCu} were proportional to c_{Cu}, then equation (7) shows that n_{CuCa} would be constant, as indicated by a continuous line in Figure 8.) The dashed lines in Figure 8 are linear fits to the data for the atom pair Ca-Cu, with the corresponding equations in Table 4. However, these linear fits are not satisfactory, firstly because the fit to n_{CaCu} becomes negative for low Cu content, and secondly because the two fits are fundamentally incorrect in that they do not obey equation (7). Furthermore, the values obtained for n_{CuCa} do not behave as expected; intuitively, direct substitution of copper for magnesium atoms should have little or no effect on the packing of calcium atoms around copper, but the fitting results indicate that, as copper atoms are added to the glass, n_{CuCa} increases. The fit to the Ca-Cu peak is the least reliable of the three copper peaks, because it is at the longest distance, and is more affected by overlap problems with longer distance peaks, such as the 'dummy' Mg-Ca peak. Therefore the values given by peak fitting should be treated with caution. However, further insight into the Ca-Cu peak may be obtained by consideration of hard sphere structural models, as discussed below.

5.2 Hard sphere calculations

In order to gain further insight into the coordination numbers and distributions of interatomic distances, and their derivation from experimental diffraction data, partial correlation functions were

calculated for the hypothetical binary hard sphere systems, $Ca_{60}Cu_{40}$ and $Ca_{60}Mg_{40}$ using the Percus-Yevick (PY) approximation [25,26]. A PY simulation of a hard sphere system is considered to be an appropriate model for the structure of this glass system because, by definition, hard spheres have no chemical interactions and hence the packing is random, in agreement with the solute-solute peak fitting results. For this consideration, the simulations are compared with only the neutron diffraction data, because of the superior real-space resolution for the neutron diffraction data.

The PY calculations directly yield partial structure factors, and these were multiplied by a Debye-Waller factor, $\exp(-u^2/2Q^2)$, to represent the effect of atomic vibrations, and then Fourier transformed (as in equation (2)), using exactly the same modification function as for the experimental data, to obtain the partial correlation functions, $t_{ll'}^{\mathrm{N}}(r)$, which describe correlations between an average origin atom of element *l*, and atoms of element *l'* at a distance *r*. For the PY calculations it is necessary to specify the composition, the hard sphere radii and the density (or packing fraction). In order to perform calculations for a hypothetical $Ca_{60}Cu_{40}$ glass, the density was estimated as 2.858 gcm^{-3} by extrapolation of the ternary densities (Table 3), leading to a packing fraction of 0.61 which was used for all the PY calculations. The pairwise sums of the hard sphere radii give the absolute lower limit of approach for the hard spheres, whereas the atomic radii given in Table 1 are related to the mean interatomic distances. Hence it is not appropriate to use the atomic radii as the hard sphere radii in the PY calculations. It was found empirically that hard sphere radii that are 6.25 % smaller than those given in Table 1 give peak positions which both approximate the interatomic distances in Table 2, and simulate the peaks in the experimental correlation functions well. An RMS thermal variation in interatomic distance, *u*, of 0.1 Å was found to give similar peak widths to the experimental data. The values in Table 3 are somewhat larger than this value, since they represent the combined effects of thermal and static disorder.

As indicated in Table 2, the Cu-X (where X is not Cu) distances in these glasses are consistent with the sum of covalent radii, whereas all other distances are consistent with the sum of metallic radii. Thus Figure 10(a) shows the PY simulation of the Cu-Cu partial correlation function, generated using metallic radii, whilst Figure 10(b) shows the PY simulation of the Ca-Cu (or Cu-Ca) partial

correlation function calculated using covalent radii. It should be acknowledged that the simulation of different partial correlation functions using different sets of radii does not correspond to a self-consistent model. However, this approach does provide a reasonable estimate of the form of the distribution of nearest neighbour interatomic distances for each pair of elements, and it also gives an estimate of longer range correlations. In particular, the first peak of each simulated partial correlation function is asymmetric with a sharper leading edge, and a broader trailing edge. This peak shape is consistent with some real-space, high resolution experimental results on the partial correlation functions for metallic glasses (for example, see reference [45]). In terms of a hard sphere model, the sharp leading edge can be interpreted as arising from spheres which are in direct contact, whilst the broad trailing edge arises from spheres which are almost touching, but are not actually in contact because their positions are constrained by all the other spheres which are packed around them. The fitting to the diffraction data of a single symmetric peak for each atom pair corresponds more closely to the contribution to the correlation function from atoms which are in direct contact. However, the traditional concept of a 'first coordination shell' may perhaps correspond more closely to the combined contributions from atoms which are almost touching, as well as those which are in direct contact. The coordination numbers for the PY simulation were evaluated in two ways: Firstly, for each atom pair, a resolution-broadened Gaussian was fitted to the leading edge of the first peak in $t_{ll'}^{\mathrm{N}}(r)$ (as shown in Figure 10), and secondly $rt_{ll'}^{\mathrm{N}}(r)$ was integrated up to the minimum after the first peak. The first approach gives a closer simulation of the way in which the experimental data were fitted, and only includes neighbours which are in close contact, whereas the second approach gives the total coordination number for the first coordination shell, for distances up to the minimum in the distribution. The coordination numbers for both approaches are given in Table 5.

The value of n_{CuCu} from the fit to the PY simulation agrees, within error (see Table 5), with the coordination number from linear extrapolation of the experimental coordination numbers, using the proportionality relation (continuous line in Figure 8). This is a further indication that the Cu-Cu peaks fitted to the glass data are an accurate representation of the close contact part of the distribution of Cu-Cu distances for randomly distributed copper atoms. The solute-solute coordination numbers, n_{jk},

derived by fitting the experimental data, have a physically reasonable behaviour, in that they are proportional to c_k, and the agreement between the extrapolation of the fit values for n_{CuCu} and the PY result is further confirmation that the values are physically reasonable. The Cu-Cu component of the fits to the experimental data is the most reliable of all components because it occurs at shortest distance, and this is why it yields reasonable, reliable results.

As noted in the previous section, the behaviour of the Ca-Cu coordination numbers obtained from fitting the data is not physically reasonable. One of the reasons for this is that the fit to the Ca-Cu peak in the experimental data is strongly affected by the relatively broad 'dummy' Mg-Ca peak (see Figures 5-7). Thus it would not be justifiable to extrapolate the values for the Ca-Cu coordination numbers in the same way as for the Cu-Cu coordination numbers, and instead a different approach was adopted. This approach is to start with the value of 3.23 for the Ca-Cu coordination number from the PY simulation for $Ca_{60}Cu_{40}$, and to extrapolate to the compositions of the glass samples on the assumption of random packing with no chemical effects. The results from this approach are shown in Figure 11 and the discrepancy between them and the experimental coordination numbers grows as the Mg content increases, due to the increasing effect from overlap with the Mg-Ca peak (see Figures 5-7). Therefore, by using the PY simulation, the more reasonable values for n_{CaCu} and n_{CuCa} have been estimated than were achievable by peak fitting. A comparison of the coordination numbers is given in Table 3.

The result for n_{CuX} calculated using the PY derived values for n_{CuCa} and n_{CaCu} is larger than measured by peakfitting, ~6.5, and does not vary significantly with composition. The results are still less than expected by the DRP and ECP models, but these results are a measurement of the symmetric distribution of the nearest neighbours only. The PY simulations indicate that the distributions of interatomic distances are likely to be asymmetric, and the coordination numbers involving copper (Table 3) are likely to be an underestimate of the true coordination numbers, due to the failure to include the broader trailing edge in the peak fitting. Table 5 shows that integrating the total area under the first peak in $t_{CuCa}(r)$, calculated by PY, gives a value for n_{CuCa} of 8.83, which is much closer to the

coordination number expected from consideration of the DRP and ECP models for binary glasses, and from the crystal Ca_2Cu.

Figure 12 shows a comparison of the experimental neutron correlation functions, $T^N(r)$, with a simulation based on the PY calculations for a hard sphere $Ca_{60}Cu_{40}$ glass. The simulated $T^N(r)$ was calculated from a sum of the partial correlation functions in which they were weighted according to the composition of each ternary glass. This makes the assumption that the coordination numbers for Cu-Cu, Cu-Ca and Ca-Ca are unchanged as Mg is substituted for Cu. In the regions of the three peaks (between 2.3 and 3.0 Å and around 4.0 Å), the simulation gives a reasonably close description of the experimental results, but the lack of correlations involving magnesium in the model leads to a lack of intensity in the region between 3 and 4 Å where Mg-Mg and Mg-Ca correlations are expected.

To improve the model, the partial correlation functions were calculated for a hypothetical $Ca_{60}Mg_{40}$ glass using the PY approximation for hard spheres. The Mg-Mg and Mg-Ca partial correlation functions from this calculation (weighted according to the composition of each ternary glass) were added to the simulation of $T^N(r)$ based on the $Ca_{60}Cu_{40}$ PY calculations (shown in Figure 12), and the results of this procedure are shown in Figure 13. Now the PY simulations reproduce the experimental peak positions, peak shapes, and longer correlations reasonably well. The peak areas are reproduced less well, but this is a consequence of the use of results from binary hard sphere simulations which leads to an overestimate of the coordination numbers; for example, in reality the replacement of Mg for some of the Cu in $Ca_{60}Cu_{40}$ will lead to a reduction in the X-Cu and X-Ca coordination numbers (as is shown by the coordination numbers in Table 3), but our simulation does not take into account this effect.

From the work presented here (and elsewhere [45]) it appears that a PY hard sphere simulation may provide a realistic prediction of the coordination numbers, and notably the distribution of interatomic distances, in metallic glasses without significant chemical ordering. However, our results concerning metallic and covalent radii (Table 2) show that it would be advantageous to have a theoretical solution of the PY equation for a binary or ternary hard sphere system in which the interatomic distances for the hard sphere cutoffs of the potentials are not additive.

6 Conclusions

A combined neutron and X-ray diffraction study has been performed for melt-spun glasses from the $Ca_{60}Mg_{40-x}Cu_x$ bulk metallic glass forming system. The correlation functions show clear evidence for solute-solute nearest neighbour interactions, unlike some diffraction studies of ternary bulk metallic glasses in the literature with lower total solute concentrations. A simple approach is developed to estimate the maximum solute atom fraction where solute-solute contact becomes topologically necessary. The Cu-Mg and Cu-Ca distances are consistent with the sum of covalent radii, whereas all other interatomic distances are consistent with the sum of metallic radii. Simultaneous fitting of multiple peaks to both neutron and X-ray correlation functions can be used to gather limited amounts of information on the structure of ternary bulk metallic glasses. Only the coordination numbers determined for Cu-Cu and Cu-Mg correlations are of reasonable reliability, due to peak overlaps for the other correlations which occur at longer distances. The Percus-Yevick (PY) approximation for binary hard sphere systems has been used to critically examine the results. This shows that the fit results for copper are a reasonable description for atoms which are in close contact but, the simulations indicate that the distributions of interatomic distances include a broader trailing edge, due to atoms which are almost touching, which is not described by the fitting of a symmetric peak. A combination of peak fitting and PY has demonstrated that copper has ~6.5 neighbours which are in close contact, but the PY simulation for $Ca_{60}Cu_{40}$ indicates that the total copper coordination number is about 12-13.

7 Acknowledgements

Neutron and X-ray experiments at the ISIS Pulsed Neutron and Muon Source were supported by a beamtime allocation (RB 820097) from the Science and Technology Facilities Council. Work at the Air Force Research Laboratory was supported through the Air Force Office of Scientific Research (Dr. Joan Fuller, Program Manager) and the Air Force on-site contract No. FA8650-10-D-5226 conducted through UES, Inc. Dayton, Ohio.

8 Tables

Atom	R_M (Å)	R_C (Å)
Ca	1.97	1.76
Mg	1.60	1.41
Cu	1.28	1.32

Table 1: The metallic [19] and covalent [20] radii for calcium, magnesium and copper.

Atom pair, *j*-*k*	r_{jk}^{M} (Å)	r_{jk}^{C} (Å)	r_{diff} (Å) (Figure 4)	Bonding
Cu-Cu	2.56	2.64	2.5	Metallic
Cu-Mg	2.88	2.73	2.7	Covalent
Cu-Ca	3.25	3.08	3.0	Covalent
Mg-Mg	3.2	2.82	—	—
Mg-Ca	3.57	3.17	3.6	Metallic
Ca-Ca	3.94	3.52	3.8	Metallic

Table 2: The closest approach of each interatomic pair, r_{jk}^{M} and r_{jk}^{C}, calculated using metallic [19] and covalent [20] radii respectively. These distances are compared to the interatomic distances, r_{diff}, determined from the composition differences shown in Figure 4, and the type of bonding for each correlation has been identified.

			$Ca_{60}Mg_{15}Cu_{25}$	$Ca_{60}Mg_{20}Cu_{20}$	$Ca_{60}Mg_{25}Cu_{15}$
Atomic pair, *j-k*	Interatomic distance, r_{jk} (Å)	Peak width, $\langle u_{jk}^2 \rangle^{½}$ (Å)	Coordination number, n_{jk}	Coordination number, n_{jk}	Coordination number, n_{jk}
Cu-Cu	2.52*	0.12*	1.18(5)	0.88(6)	0.74(6)
Cu-Mg	2.73*	0.18*	0.51(8)	0.77(4)	0.92(5)
Cu-Ca	3.04*	0.15*	4.05(4) *[4.85]*	3.56(6) *[4.85]*	3.08(6) *[4.85]*
Mg-Cu	2.73*	0.18*	0.9(1)	0.77(4)	0.55(3)
Ca-Cu	3.04*	0.15*	1.69(7) *[2.02]*	1.19(6) *[1.62]*	0.77(3) *[1.21]*
Total Cu coordination number			5.74(9) *[6.54]*	5.21(8) *[6.50]*	4.74(8) *[6.51]*
Density (g cm^{-3})			2.367(1)	2.200(1)	2.039(1)

Table 3: The fitted parameters for the copper correlations in the three glasses. The interatomic distances were fixed for all three samples. The peak widths were allowed to vary for the $Ca_{60}Mg_{15}Cu_{25}$ sample, and were subsequently fixed. Values given in square brackets and italics are calculated from the PY simulation for $Ca_{60}Cu_{40}$.

Atomic pair	Gradient	Intercept
Ca-Cu	0.090 ± 0.007	-0.59 ± 0.12
Cu-Ca	0.097 ± 0.007	1.62 ± 0.15

Table 4: Linear fits to the dependence on Cu content of coordination number data (Figure 8).

Atomic pair, *j-k*	n_{jk} from extrapolation of parameters from peak fits to experimental data (with errors)	n_{jk} from PY peak fit	n_{jk} from PY integration
Cu-Cu	1.87 (12)	1.77	3.82
Cu-Ca	5.50 (32)	4.85	8.83
Ca-Cu	3.05 (30)	3.23	5.89
Cu-Cu + Cu-Ca	7.37	6.62	12.65

Table 5: The Cu-Cu, Cu-Ca and Ca-Cu coordination numbers for $Ca_{60}Cu_{40}$, obtained by linear extrapolation of the results from peak fitting the experimental data for ternary glasses. These are compared with values obtained from PY binary hard sphere simulations of the partial correlation functions of $Ca_{60}Cu_{40}$ by peak fitting and by integration (see text for details).

9 Figures

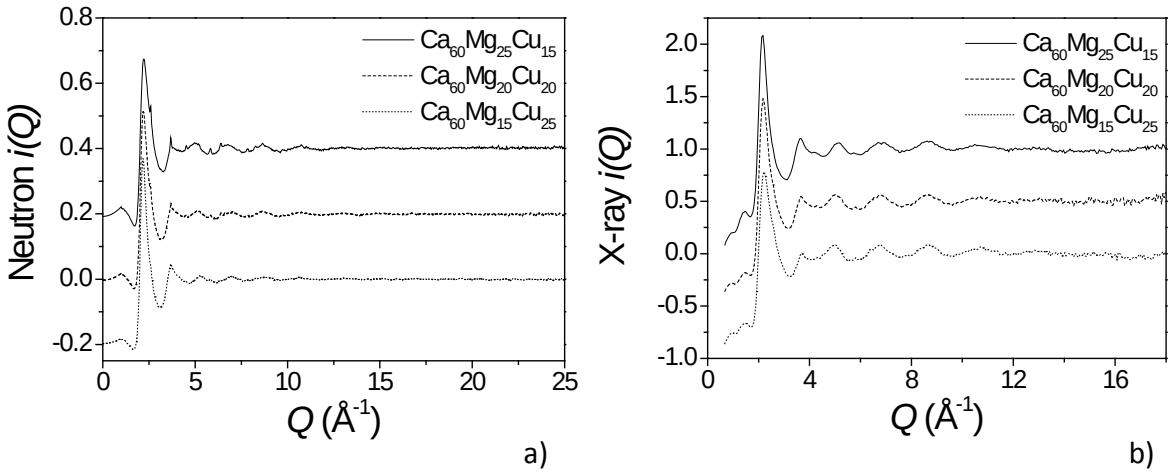

Figure 1: Distinct scattering data for three glass compositions measured using a) neutrons and b) X-rays.

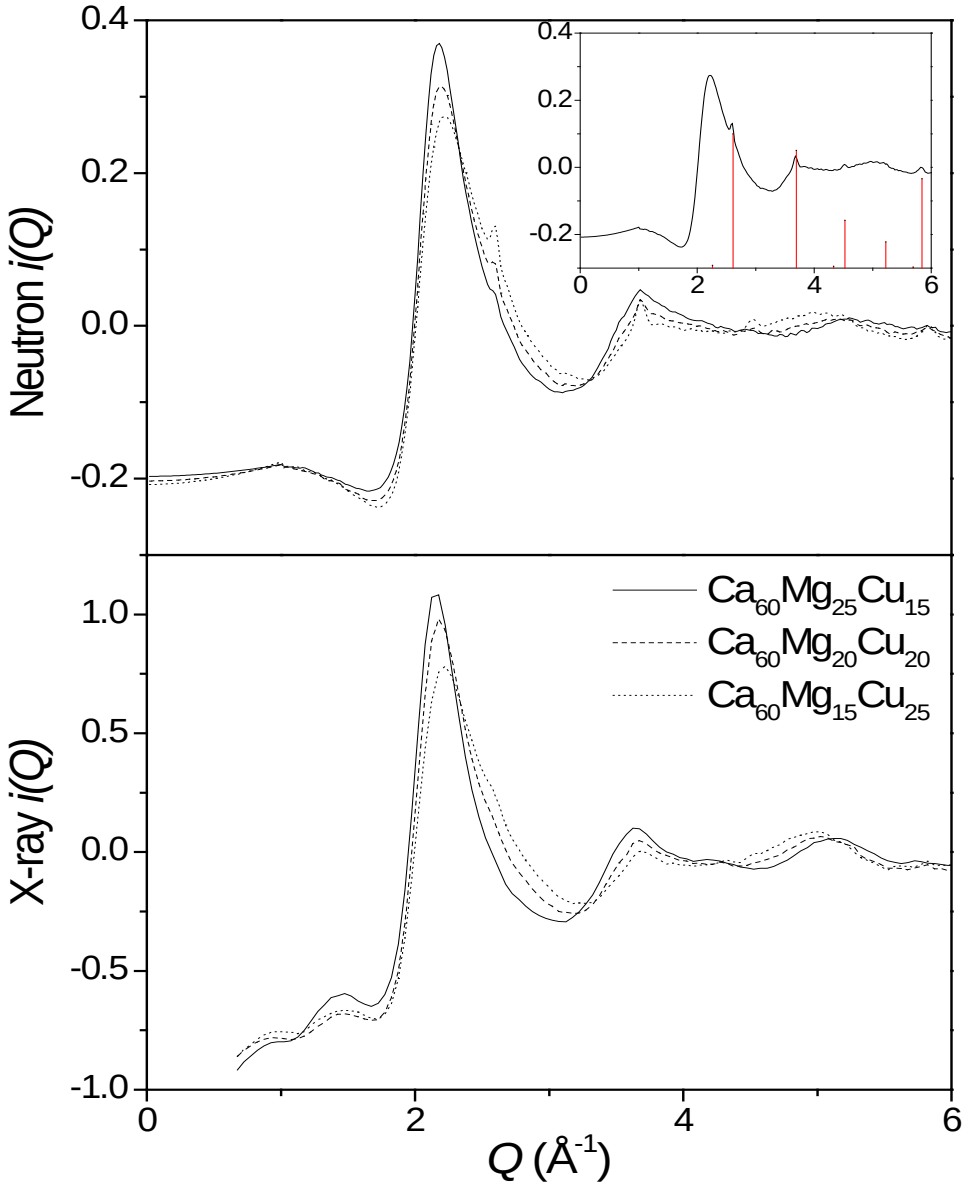

Figure 2: A comparison of the low-*Q* region of *i*(*Q*) for the three samples. Inset is a comparison of the neutron diffraction data for $Ca_{60}Mg_{15}Cu_{25}$ and the Bragg peaks expected for CaO [38].

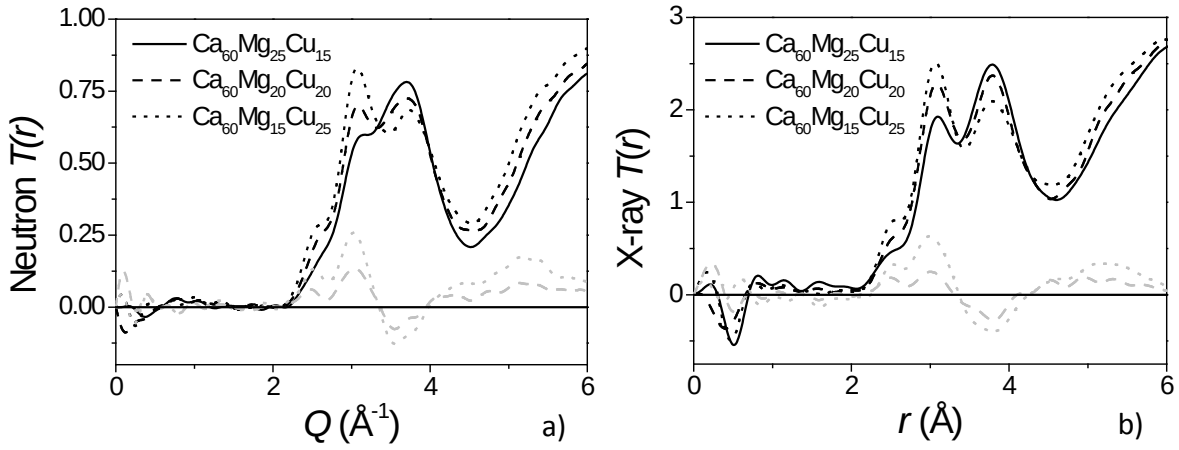

Figure 3: The total correlation function measured with neutrons (a) and X-rays (b). The differences are also shown, where the dashed grey line is the difference $Ca_{60}Mg_{15}Cu_{25}$-$Ca_{60}Mg_{20}Cu_{20}$ and the grey dotted line is the difference $Ca_{60}Mg_{15}Cu_{25}$-$Ca_{60}Mg_{25}Cu_{15}$.

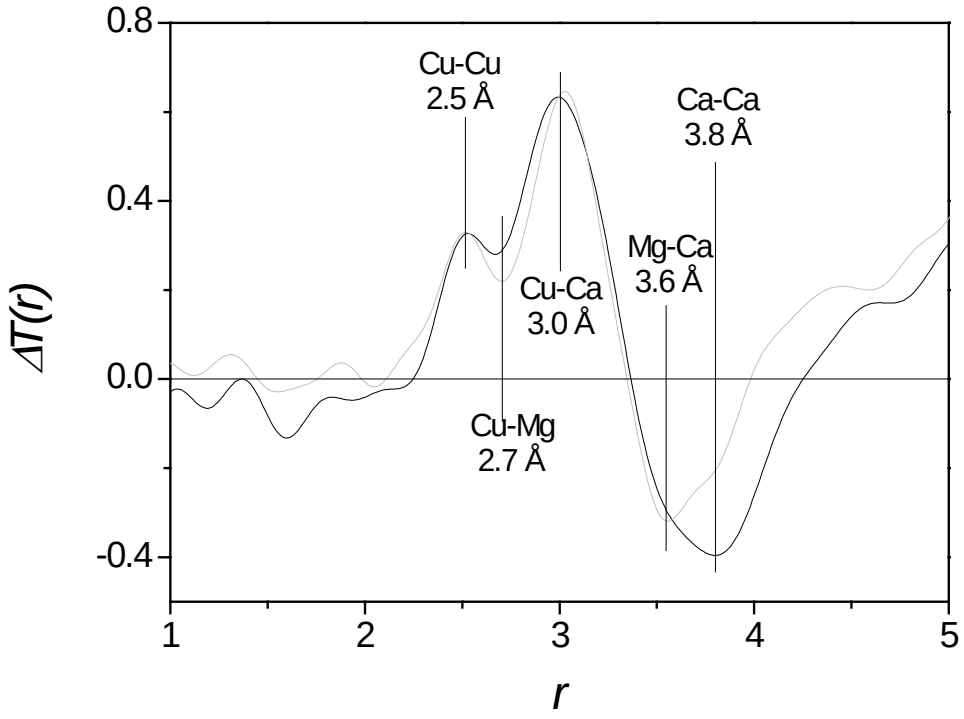

Figure 4: Differences between the total correlation functions of the two most disparate compositions ($Ca_{60}Mg_{15}Cu_{25}$ − $Ca_{60}Mg_{25}Cu_{15}$) for neutrons (grey) and X-rays (black). The neutron difference has been multiplied by 2.5 to be comparable with the X-ray data.

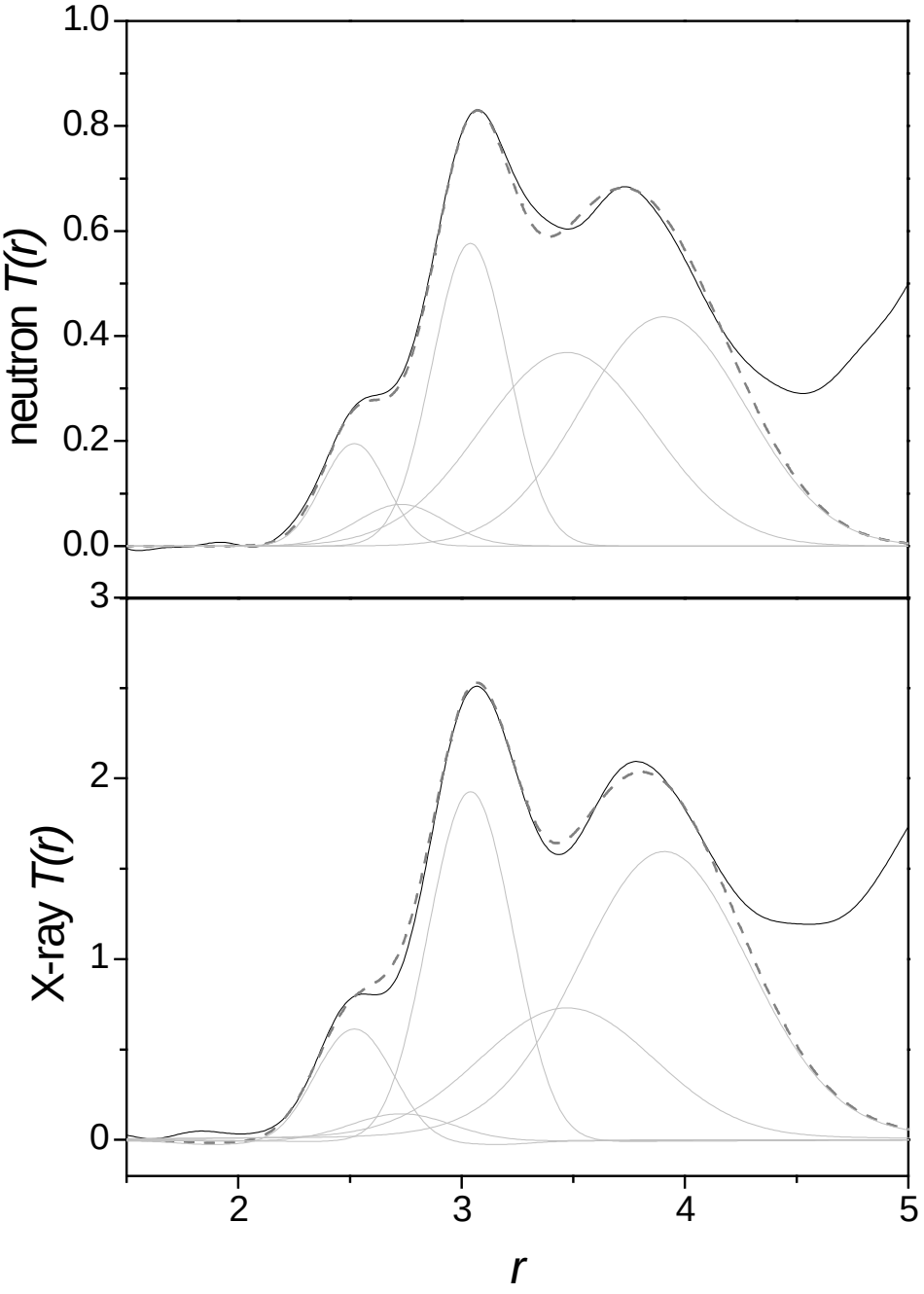

Figure 5: Fits to x-ray and neutron correlation functions for $Ca_{60}Mg_{15}Cu_{25}$. (The continuous line shows the experimental data, whilst the dashed line shows the fitted function, and the dotted lines show the components of the fit).

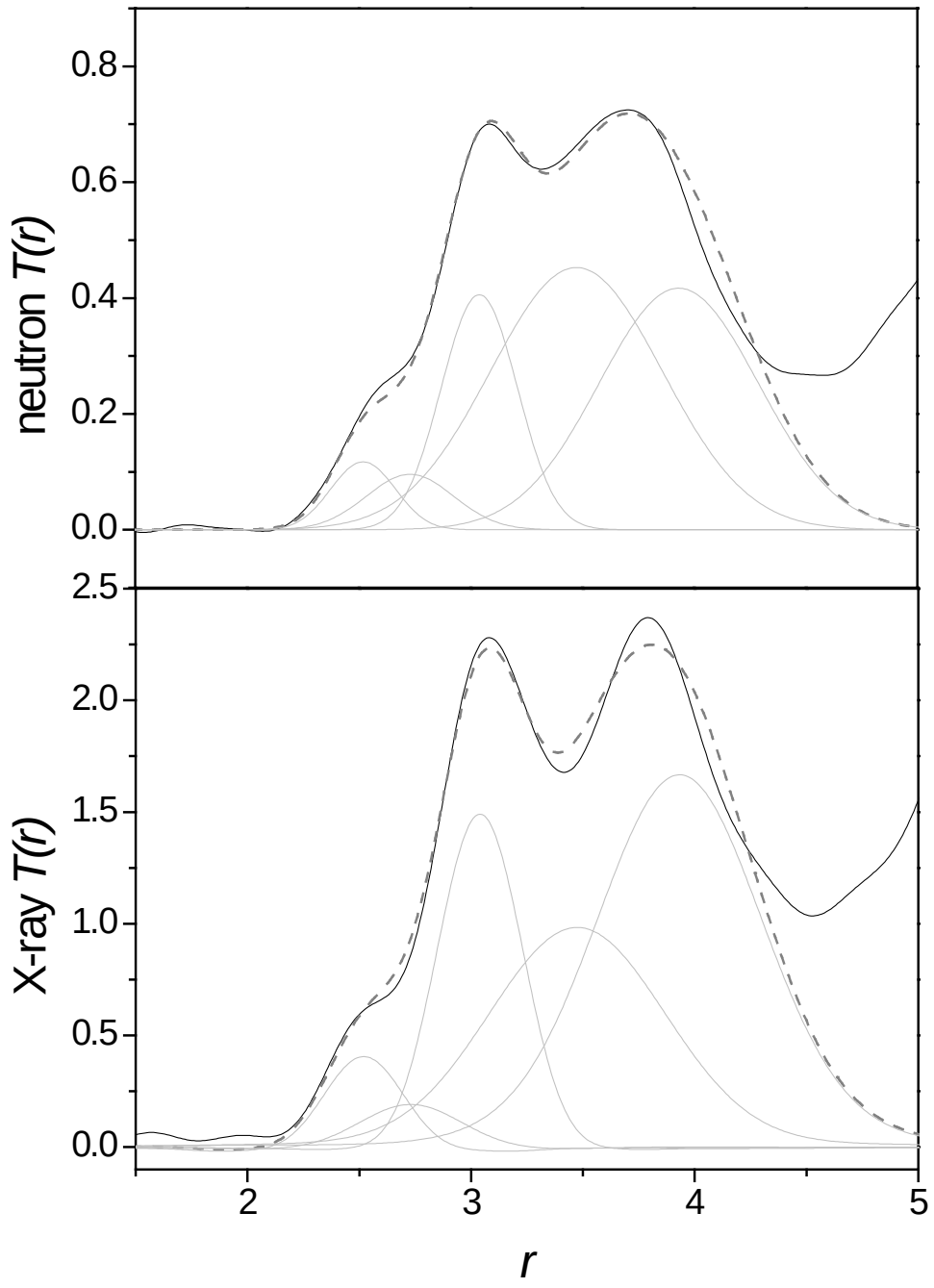

Figure 6: Fits to x-ray and neutron correlation functions for $Ca_{60}Mg_{20}Cu_{20}$. (The continuous line shows the experimental data, whilst the dashed line shows the fitted function, and the dotted lines show the components of the fit).

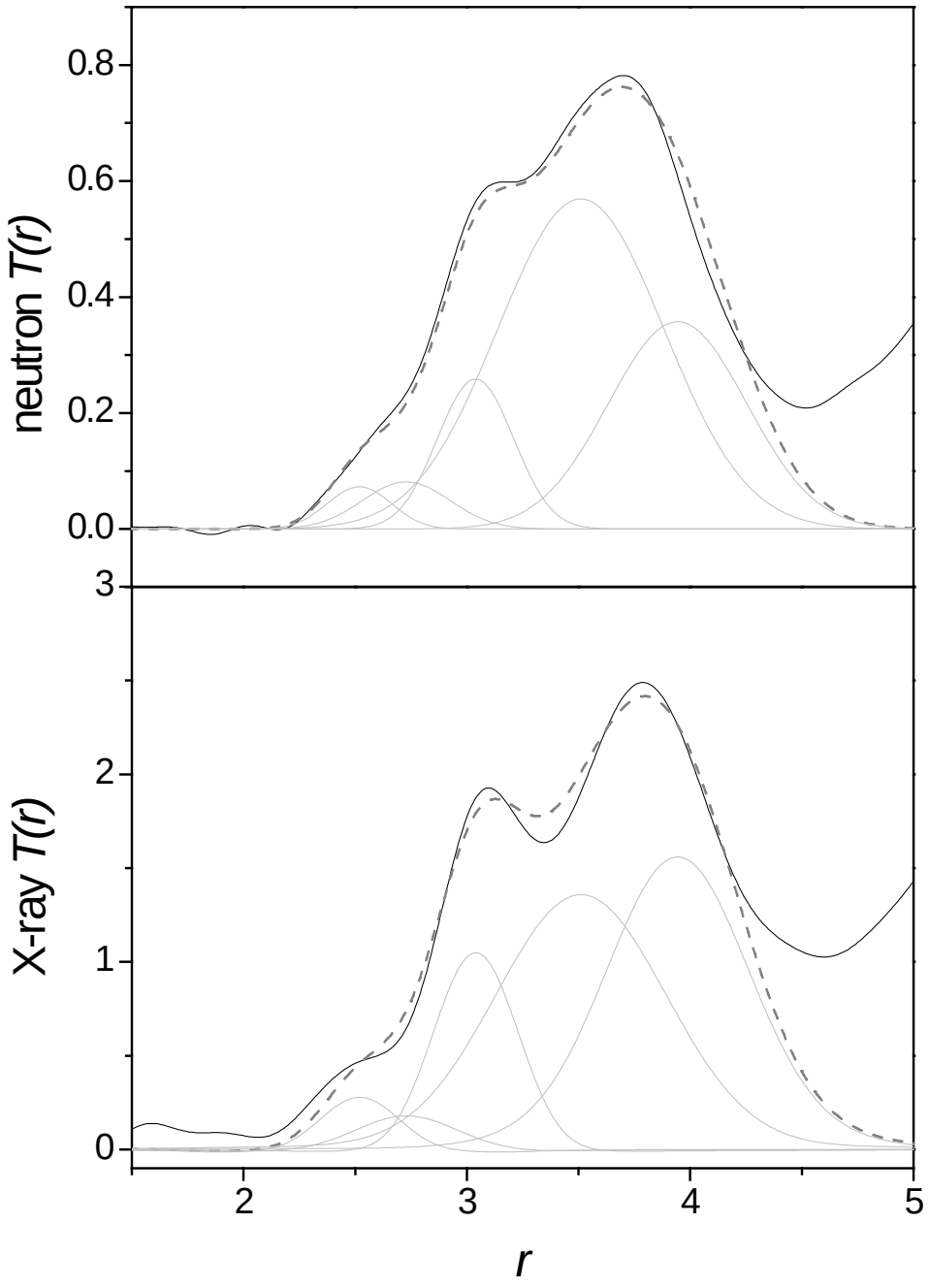

Figure 7: Fits to x-ray and neutron correlation functions for $Ca_{60}Mg_{25}Cu_{15}$. (The continuous line shows the experimental data, whilst the dashed line shows the fitted function, and the dotted lines show the components of the fit).

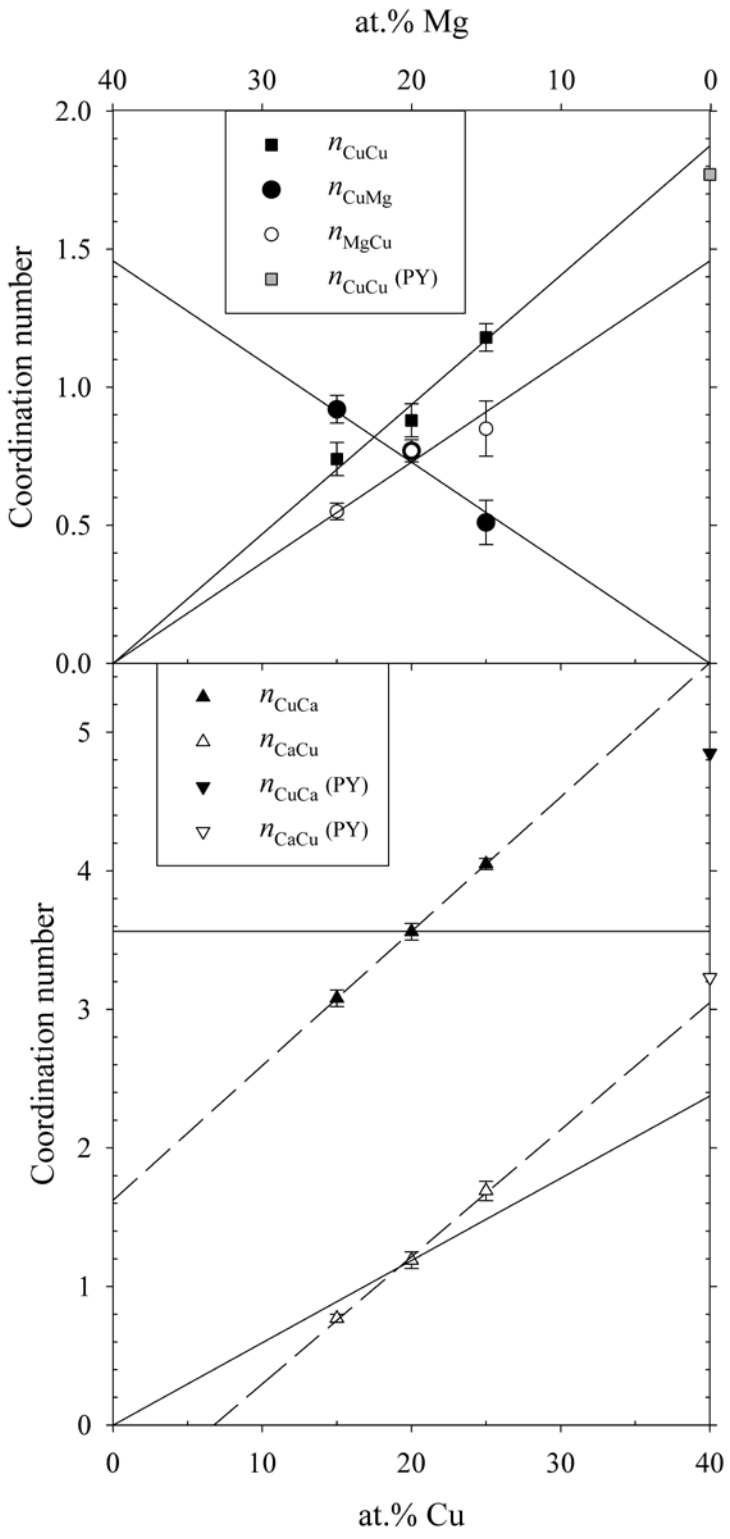

Figure 8: Cu coordination numbers, with closed symbols indicating Cu-X, and open symbols indicating X-Cu. Squares are Cu-Cu, circles are Cu-Mg (and Mg-Cu) and triangles are Cu-Ca (and Ca-Cu). The continuous lines are fits of the form n_{jk}=constant×c_k, whilst the dashed lines are linear fits. The symbols (labelled PY) at 40 at.% Cu indicate the coordination numbers obtained by fitting resolution-broadened Gaussians to the Cu-Ca, Ca-Cu and Cu-Cu partial correlation functions calculated for the binary glass $Ca_{60}Cu_{40}$ using the Percus-Yevick hard sphere approximation.

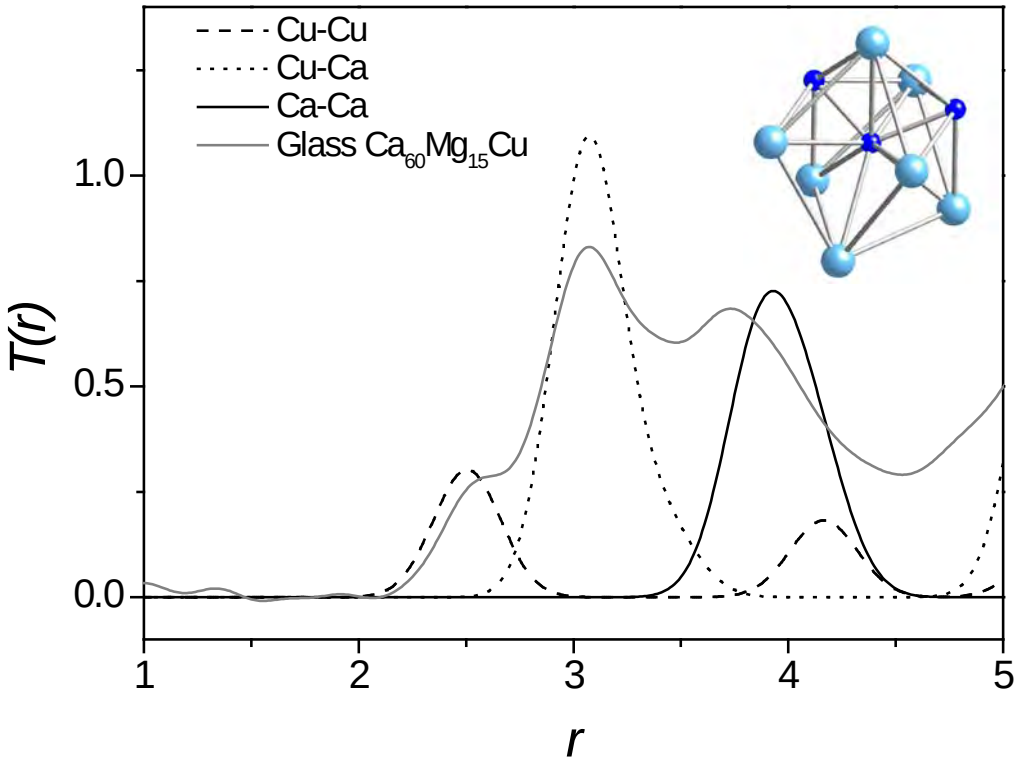

Figure 9: A comparison the experimental $T^{N}(r)$ for $Ca_{60}Mg_{15}Cu_{25}$ with the Cu-Cu, Cu-Ca and Ca-Ca contributions simulated (see text for details) according to the Ca_2Cu crystal structure [42]. The inset shows the atomic arrangement around a Cu atom in the crystal, including all atoms closer than 3.5 Å (small spheres are Cu, large spheres are Ca).

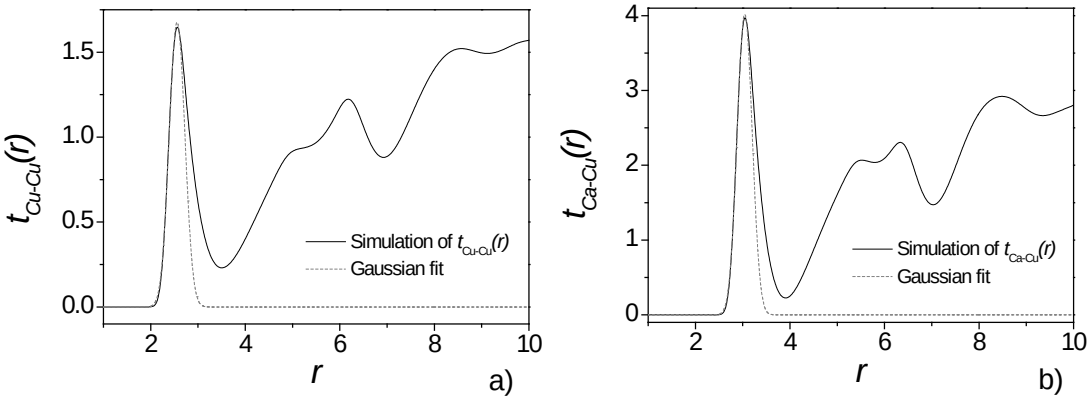

Figure 10: Partial correlation functions, $t_{jk}^{N}(r)$, calculated using the Percus-Yevick approximation for a binary hard sphere system, showing a) the Cu-Cu function, and b) the Cu-Ca function, with fits to the leading edge of a resolution-broadened Gaussian.

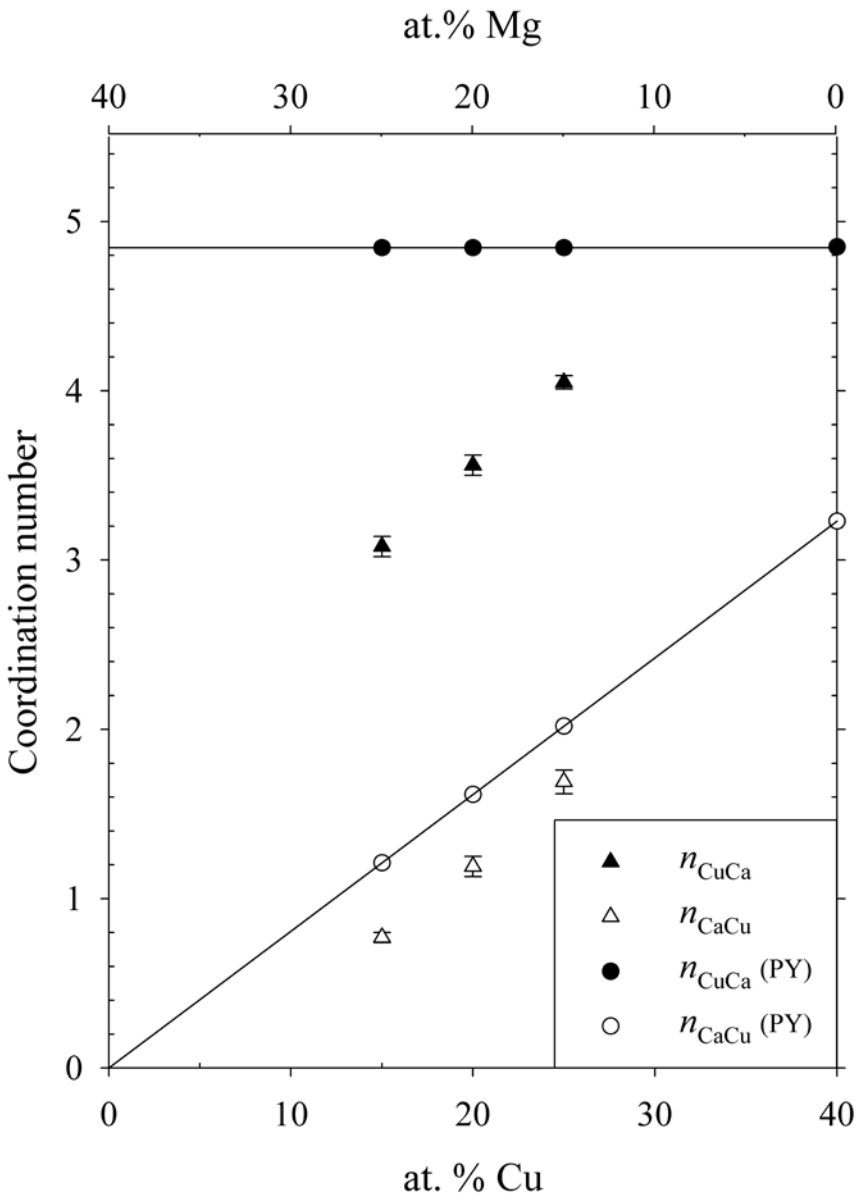

Figure 11: n_{CaCu} and n_{CuCa} predicted on the basis of the PY simulation for $Ca_{60}Cu_{40}$ and assuming random packing with no chemical effects (circles), together with the results from fitting the experimental data (triangles). The lines show the composition-dependence of the coordination numbers according to this approach.

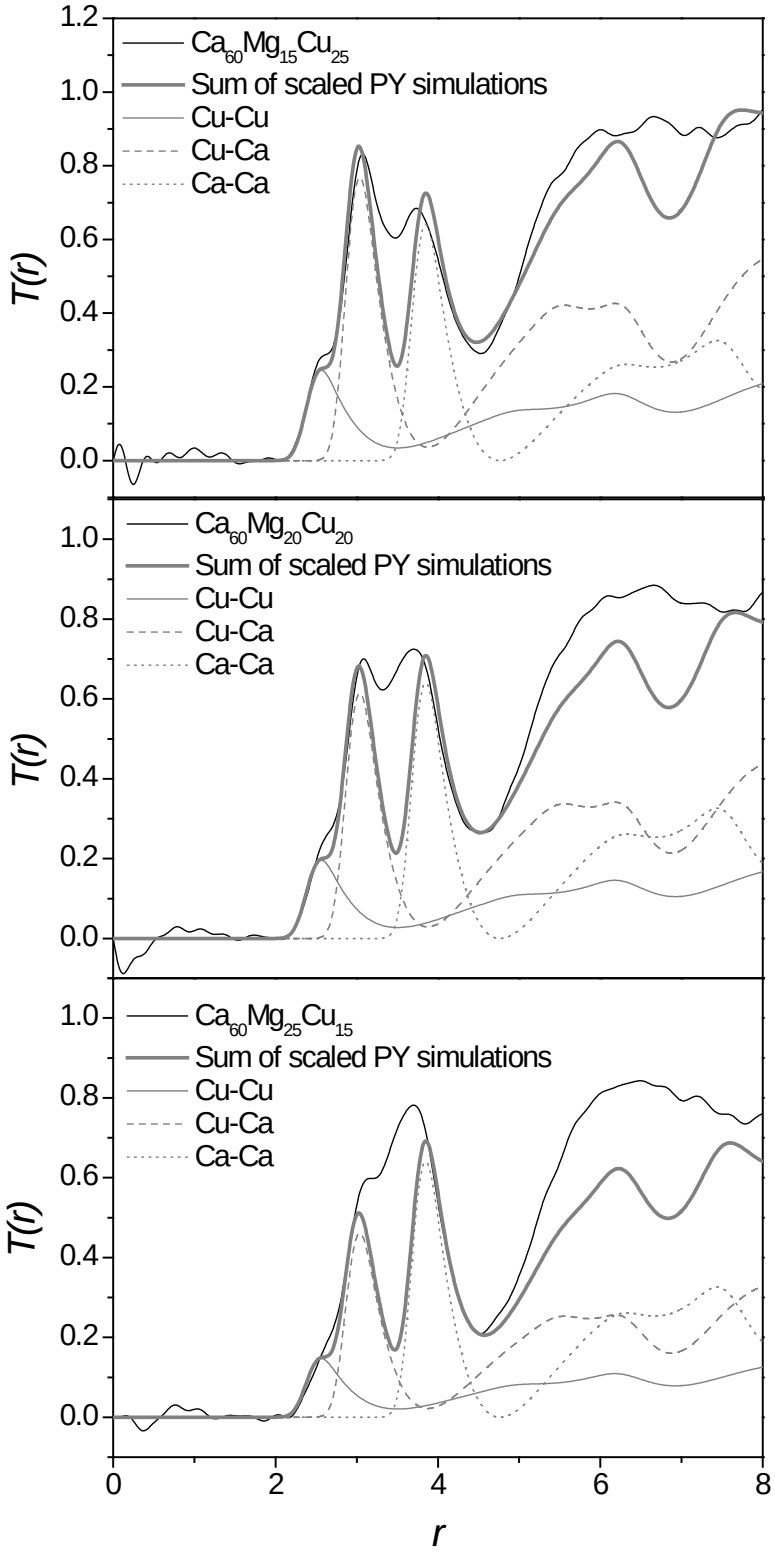

Figure 12: A comparison of $T^{N}(r)$ for the three glasses with a simulation based on the hard sphere PY calculations for $Ca_{60}Cu_{40}$ (see text for details).

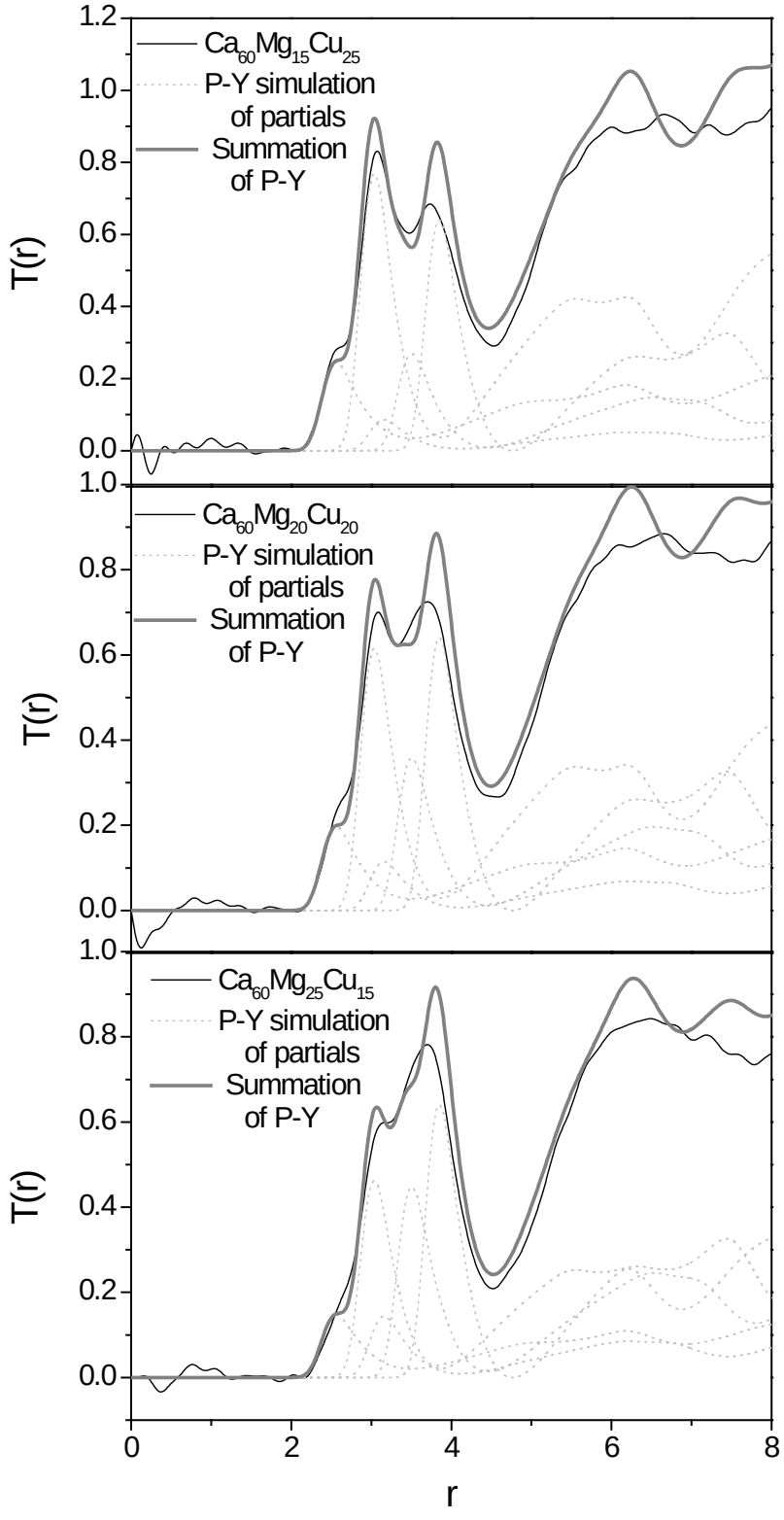

Figure 13: A comparison of $T^N(r)$ for the three glasses with a simulation based on a combination of the hard sphere PY calculations for $Ca_{60}Cu_{40}$ and for $Ca_{60}Mg_{40}$ (see text for details).

10 References

1. W. Klement, R.H. Willens and P. Duwez, Nature 187(1960)869.
2. J.A. Wert, C. Thomsen, R.D. Jensen and M. Arentoft, J. Mater. Process. Technol. 209(2009)1570.
3. W.H. Wang, C. Dong and C.H. Shek, Mat. Sci. Eng. R 44(2004)45.
4. P. Lamparter, W. Sperl and S. Steeb, Z. Naturforsch. 37a(1982)1223.
5. D.B. Miracle, Acta Mater. 54(2006)4317.
6. E. Nold, P. Lamparter, H. Olbrich, G. Rainer-Harbach and S. Steeb, Z. Naturforsch. 36a(1981)1032.
7. P. Lamparter, A. Habenschuss and A.H. Narten, J. Non-Cryst. Solids 86(1986)109.
8. A. Sadoc and J. Dixmier, J. Mater. Sci. 23(1976)187.
9. D.B. Miracle, D. Louzguine-Luzgin, L. Louzguina-Luzgina and A. Inoue, Int. Mater. Rev. 55(2010)218.
10. W.H. Wang, Q. Wei, S. Friedrich, M.P. Macht, N. Wanderka and H. Wollenberger, Appl. Phys. Lett. 71(1997)1053.
11. W.-H. Wang, Q. Wei and S. Friedrich, Phys. Rev. B 57(1998)8211.
12. O.N. Senkov and J.M. Scott, Mater. Lett. 58(2004)1375.
13. O.N. Senkov, J.M. Scott and D.B. Miracle, J. Alloys Compd. 424(2006)394.
14. O.N. Senkov and J.M. Scott, J. Non-Cryst. Solids 351(2005)3087.
15. O.N. Senkov, D.B. Miracle and J.M. Scott, Intermetallics 14(2006)1055.
16. O.N. Senkov, D.B. Miracle, E.R. Barney, A.C. Hannon, Y.Q. Cheng and E. Ma, Phys. Rev. B 82(2010)104206.
17. A. Inoue, Mat. Sci. Eng. A 226-228(1997)357.
18. A. Peker and W.L. Johnson, Appl. Phys. Lett. 63(1993)2342.
19. N.N. Greenwood and A. Earnshaw, Chemistry of the Elements 2nd Ed, Butterworth-Heinemann, Oxford, 1997.
20. B. Cordero, V. Gómez, A.E. Platero-Prats, R. Revés, J. Echeverría, E. Cremades, F. Barragán and S. Alvarez, Dalton Trans. (2008)2832.
21. H.Y. Hsieh, B.H. Toby, T. Egami, Y. He, S.J. Poon and G.J. Shiflet, J. Mater. Res. 5(1990)2807.
22. H.Y. Hsieh, T. Egami, Y. He, S.J. Poon and G.J. Shiflet, J. Non-Cryst. Solids 135(1991)248.
23. J. Saida, T. Sanada, S. Sato, M. Imafuku, E. Matsubara and A. Inoue, J. Alloys Compd. 434-435(2007)135.
24. J. Saida, M. Imafuku, S. Sato, T. Sanada, E. Matsubara and A. Inoue, Mat. Sci. Eng. A 449-451(2007)90.
25. N.W. Ashcroft and D.C. Langreth, Phys. Rev. 156(1967)685.
26. J.E. Enderby and D.M. North, Phys. Chem. Liq. 1(1968)1.
27. A.C. Wright, J. Non-Cryst. Solids 112(1989)33.
28. A.L. Patterson, Z Kristallogr 90(1935)517.
29. A.K. Soper, J. Phys.: Condens. Matter 19(2007)335206.
30. P.G. Mikolaj and C.J. Pings, Phys. Chem. Liq. 1(1968)93.
31. P.J. Black and J.A. Cundall, Acta Cryst. 19(1965)807.
32. A.C. Hannon, Nucl. Instrum. Meth. A 551(2005)88.
33. A.K. Soper, *Gudrun software*: http://www.isis.stfc.ac.uk/instruments/sandals/data-analysis/gudrun8864.html.
34. A.C. Hannon, W.S. Howells and A.K. Soper, IOP Conf. Ser. 107(1990)193.
35. A.K. Soper, *GudrunX software*: http://www.isis.stfc.ac.uk/support-laboratories/xrd/data-analysis/xrd-data-analysis9203.html.
36. R.M. Moss, *PhD Thesis*. 2009, University of Kent.
37. E. Lorch, J. Phys. C 2(1969)229.
38. A. Stergiou, I. Kerasiotis and C. Stergiou, J. Optoelectron. Adv. Mater. 9(2007)1772.

39. D.B. Miracle, D. Louzguine-Luzgin, L. Louzguina-Luzgina and A. Inoue, Int. Mater. Rev. 55(2010)218.
40. T. Egami and V. Vitek, in Amorphous Materials, edited by V. Vitek (Metal Society of AIME, Warrendale, PA, 1983), p. 127
41. T. Egami and S. Aur, J. Non-Cryst. Solids 89(1987)60.
42. M. Fornasini, Acta Cryst. B 38(1982)2235.
43. Y.Q. Cheng, E. Ma and H.W. Sheng, Phys. Rev. Lett. 102(2009)245501.
44. A.C. Hannon, Rutherford Appleton Laboratory Report RAL-93-063, 1993.
45. A.C. Hannon, A.C. Wright and R.N. Sinclair, Mat. Sci. Eng. A 134(1991)883.